Introduction to Fracture Mechanics

2

2.1 Introduction

The theory of elasticity used in Chap. 1 served the purpose of illustrating the close form of analytical procedures in order to develop constitutive equations for predicting failure of crack-free solids [1]. However, when solids contain flaws or cracks, the field equations are not completely defined by the theory of elasticity since it does not consider the stress singularity phenomenon near a crack tip. It only provides the means to predict general yielding as a failure criterion. Despite the usefulness of predicting yielding, it is necessary to use the principles of fracture mechanics to predict failure of solid components containing cracks.

Fracture mechanics is the study of mechanical behavior of cracked materials subjected to an applied load. In fact, Irwin [2] developed the field of fracture mechanics using the early work of Inglis [3], Griffith [4], and Westergaard [5]. Essentially, fracture mechanics deals with the irreversible process of rupture due to nucleation and growth of cracks. The formation of cracks may be a complex fracture process, which strongly depends on the microstructure of a particular crystalline or amorphous solid, applied loading, and environment. The microstructure plays a very important role in a fracture process due to dislocation motion, precipitates, inclusions, grain size, and type of phases making up the microstructure. All these microstructural features are imperfections and can act as fracture nuclei under unfavorable conditions. For instance, *brittle fracture* is a low-energy process (low-energy dissipation), which may lead to catastrophic failure without warning since the crack velocity is normally high. Therefore, little or no plastic deformation may be involved before separation of the solid. On the other hand, *ductile fracture* is a high-energy process in which a large amount of energy dissipation is associated with a large plastic deformation before crack instability occurs. Consequently, slow crack growth occurs due to strain hardening at the crack tip region.

N. Perez, *Fracture Mechanics*, DOI 10.1007/978-3-319-24999-5_2

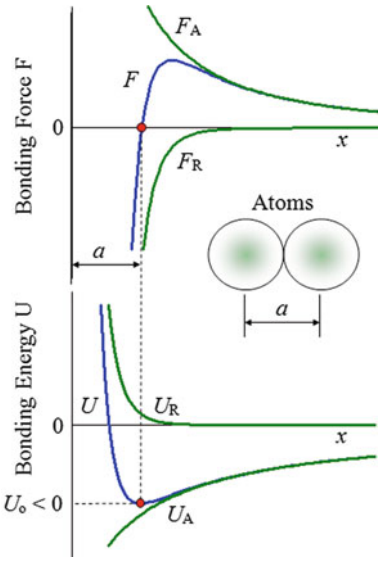

Fig. 2.1 Sinusoidal stress vs. interatomic displacement

2.2 Theoretical Strength

Consider the predicament of how strong a perfect (ideal) crystal lattice should be under an applied state of stress and the comparison of the actual and theoretical strength of metals. This is a very laborious work to perform, but theoretical approximations can be made in order to determine or calculate the stress required for fracture of atomic bonding in crystalline or amorphous crystals.

Assume a simple sinusoidal stress-displacement law with a half period of $\lambda/2$ shown in Fig. 2.1 which predicts the simultaneous separation of atoms when the atomic separation reaches a critical value.

For an ideal crystal subjected to a tensile load and a shear load, which generates small displacements, the sinusoidal stress functions are

$$\sigma = \sigma_{\max} \sin\left(\frac{2\pi x}{\lambda}\right) \simeq \left(\frac{2\pi x}{\lambda}\right) \sigma_{\max} \tag{2.1a}$$

$$\tau = \tau_{\max} \sin\left(\frac{2\pi x}{a_o}\right) \simeq \left(\frac{2\pi x}{a_o}\right) \tau_{\max} \tag{2.1b}$$

Thus, the maximum theoretical tensile and shear stresses become

$$\sigma_{\max} = \left(\frac{\lambda}{2\pi x}\right) \sigma \tag{2.2a}$$

$$\tau_{\max} = \left(\frac{a_o}{2\pi x}\right) \tau \tag{2.2b}$$

Table 2.1 Theoretical and experimental fracture strength [6]

Material	E (MPa)	$\sigma_{\max}$-Eq. (2.4)	σ_f-Exp.	$\sigma_{\max}/\sigma_f$
Silica fibers	97.10	30.90	24.10	1.28
Iron whisker	295.20	94.00	13.10	7.18
Silicon whisker	165.70	52.70	6.50	8.11
Alumina whisker	496.20	158.00	15.20	10.39
Ausformed steel	200.10	63.70	3.10	20.55
Piano wire	200.10	63.70	2.80	22.75

The interpretation of Fig. 2.1 is that the strength to pull atoms apart increases with increasing atomic distance, reaches a maximum strength (peak strength) equals to the theoretical (cohesive) tensile strength $\sigma_{\max} = \sigma_c$, and then decreases as atoms are further apart in the direction perpendicular to the applied stress. Consequently, atomic planes separate and the material cleaves perpendicularly to the tensile stress.

Assuming an elastic deformation process, Hooke's law gives the tensile modulus and the shear modulus of elasticity defined by

$$E = \frac{Tensile\ Stress}{Strain} = \frac{\sigma}{x/a_o} \tag{2.3a}$$

$$G = \frac{Shear\ Stress}{Strain} = \frac{\tau}{x/a_o} \tag{2.3b}$$

where $a_o = \lambda/2 =$ Equilibrium atomic distance (Fig. 2.1)

Combining Eqs. (2.2) and (2.3) yields the theoretical fracture strength of solid materials

$$\sigma_{\max} = \frac{E}{\pi} \tag{2.4}$$

$$\tau_{\max} = \frac{G}{2\pi} \tag{2.5}$$

Table 2.1 contains theoretical and experimental data for some elastic materials tested in tension.

The discrepancy between $\sigma_{\max}$ and σ_f values is due to the fact that the sinusoidal model assumes a concurrent fracture of atomic bonding until the atomic planes separate and σ_f is associated with plastic flow and dislocation motion. Physically, the discrepancy is due to the presence of small flaws or cracks on the surface or within the material.

Using the energy at fracture for a tension test, the fracture work per unit area can be defined by a simple integral

$$W' = \int_o^{\lambda/2} \sigma_{\max} \sin\left(\frac{\pi x}{\lambda/2}\right) dx = \left(\frac{\lambda}{\pi}\right) \sigma_{\max} \tag{2.6}$$

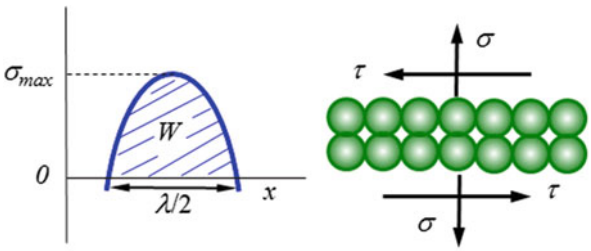

Fig. 2.2 Schematic variation of bonding force and bonding energy as functions of interatomic spacing x

Letting $2\gamma = W'$ be the total surface energy required to form two new fracture surfaces and combining Eqs. (2.4) and (2.6) yields the theoretical tensile strength in terms of surface energy and equilibrium spacing

$$\sigma_c = \sqrt{\frac{E\gamma}{a_o}} \tag{2.7}$$

In addition, the atomic bonding in solids is related to bonding forces and energies. In fact, the atomic bonding is due to repulsive and attractive forces that keep the atoms together to form symmetrical arrays. These forces as well as the potential energies depend on the interatomic spacing or distance between adjacent atoms. Figure 2.2 schematically shows the forces and the energies as functions of interatomic spacing (separation distance between centers of two atoms) for two ideal atoms. In general, atoms are considered spherical electric structures having diameters in the order of 0.1 nm. According to the theoretical plot depicted in Fig. 2.2, both attractive and repulsive forces act together to keep the atoms at their equilibrium spacing. These forces depend on temperature and pressure. The general form of the potential or bonding energy (U) and the net force (F) are defined by

$$U = \frac{C_R}{x^n} - \frac{C_A}{x^m} = U_R + U_A \tag{2.8}$$

$$F = \frac{dU}{dx} = F_R + F_A \tag{2.9}$$

where $x =$ Interatomic distance
$U_R =$ Repulsive energy
$U_A =$ Attractive energy
$F_R =$ Repulsive forces
$F_A =$ Attractive force
$C_R, C_A =$ Constants
$n, m =$ Exponents

The curves in Fig. 2.2 are known as Condon-Morse curves and are used to explain the physical events of atomic displacement at a nanoscale. At equilibrium, the minimum potential energy and the net force are dependent of the interatomic spacing; that is,

$$U_o = f(a_o) < 0 \text{ and } F = g(a_o) = 0 \tag{a}$$

However, if the interatomic spacing (a_o) is slightly perturbed elastically by the action of an applied load, a repulsive force builds up if $x < a_o$ or an attractive force builds up if $x > a_o$. Once the applied load is removed, the two atoms have the tendency to return to their equilibrium position at $x = a_o$

Conclusively, an array of atoms form a definite atomic pattern with respect to their neighboring atoms, and as a result, all atoms form a specific space lattice consisting of unit cells, such as body-centered cubic (BCC), hexagonal, monoclinic, and the like.

The reason atoms form a space lattice consisting of a unique atomic structure is due to the attractive and repulsive atomic forces being equal, but opposite in sense. Hence, the atoms are considered to be in their equilibrium state forming a particular structure. Thus, atoms are then bonded in a sea of electrons, forming metallic bonding. X-ray diffraction technique is used to reveal the type metallic structures. There are 7 types of crystal structures and 14 possible lattice geometries called Bravais lattices.

Any elastic perturbation of the lattice structure due to an external loading mode induces atomic deformation defined as the deformation strain (ϵ_x), which can be defined as a fractional change in the atomic spacing x (Fig. 2.2). Hence, $\epsilon_x = (x - a)/a$, x is the strained spacing.

Furthermore, Eq. (2.8) resembles the Lennard-Jones potentials [7] used to treat gases, liquids, and solids. There are other interatomic potential functions based on the quantum mechanical treatment of many particles. Among many references available in the literature, the book written by Michael Rieth [7] includes significant theoretical details for determining the potential energy for atomic interactions. This book includes the Buckingham, the Morse, the Lennard-Jones potentials and the Schommers potentials for aluminum, and so forth.

The most common Lennard-Jones potentials for materials 1 and 2 are of the form

$$U = 4\epsilon \left[\left(\frac{C}{x} \right)^{12} - \left(\frac{C}{x} \right)^{6} \right] \tag{2.9a}$$

where the potential ϵ and the constant C are defined by the Lorentz-Berthelot mixing rules [7]

$$\epsilon = \epsilon_{12} = \sqrt{\epsilon_1 \epsilon_2} \tag{2.9b}$$

$$C = C_{12} = \frac{C_1 + C_2}{2} \tag{2.9c}$$

These variables are just empirical correction factors.

2.3 Stress Concentration Factor

Generally, structural components subjected to external loads should be analyzed or examined by determining the stress distribution on the loaded area and the theoretical stress concentration factor (K_t) at particular point about a notch with a radius of curvature (ρ). This can be accomplished by using a suitable Airy stress function ϕ or any other appropriate function. This section partially illustrates the methodology for determining the circumferential stress component in elliptical coordinates and K_t in infinite flat plates containing circular and elliptical holes. This is purposely done prior to the introduction of fracture mechanics in order for the reader to have a basic understanding of singular stress fields in components having notches instead of cracks.

Symmetric Elliptical Hole in an Infinite Plate Consider an infinite plate containing an elliptical hole with major axis 2a and minor axis 2b as shown in Fig. 2.3, where the elliptical and Cartesian coordinates are (ξ, ψ) and (x, y), respectively. It is assumed that the flat plate has uniform dimensions and contains a through-thickness smooth elliptical hole, which is symmetric about its center. The equation of the elliptical curve can be represented by $f_\xi(x, y) = \xi$ and the one for a hyperbola is $f_\psi(x, y) = \psi$, where ξ and ψ are constants [8].

The equation of an ellipse in Cartesian coordinates is given by

$$\frac{x^2}{a^2} + \frac{y^2}{b^2} = 1 \tag{2.10}$$

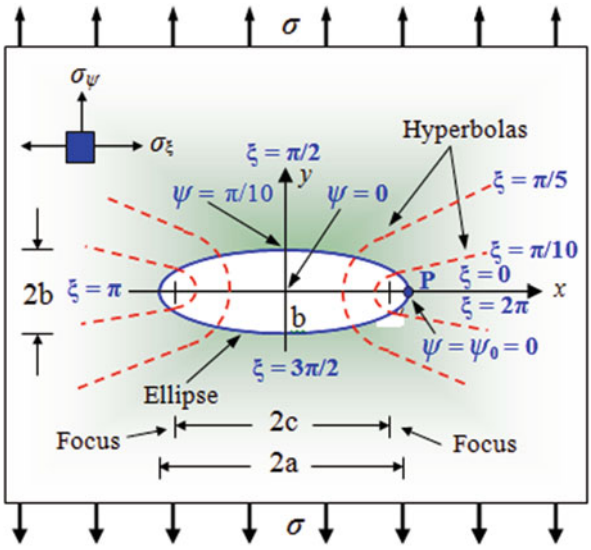

Fig. 2.3 Elliptic coordinates in an infinite plate

where

$$x = c\cosh\xi\cos\psi \tag{2.11a}$$

$$y = c\sinh\xi\sin\psi \tag{2.11b}$$

$$x + iy = c\cosh(\xi + i\psi) \tag{2.11c}$$

and

$$a = c\cosh(\xi_o) \tag{2.12a}$$

$$b = c\sinh(\xi_o) \tag{2.12b}$$

Here, the foci of the ellipse is at $x = \pm 2c$ which becomes the crack length when $\xi_o \to 0$ and $b \to 0$. In fact, the foci always lie on the major (longest) axis, spaced equally on each side of the center of the ellipse. The radius of the ellipse at the end of the major x-axis (point "P" in Fig. 2.3) is

$$\rho = \frac{b^2}{a} \tag{2.13}$$

Now, it is desirable to derive the maximum circumferential or tangential elastic stress component at an elliptical hole tip along the major axis $2a$ and the minor axis $2b$ [9]. Denote that and elliptical home becomes an elliptical crack if $2b \to 0$. Nevertheless, Inglis [3] derived the elastic stress distribution in an infinite plate subjected to a remote tension stress perpendicular to the major axis $2a$ of a flat plate. It was assumed that the plate width and height were $B >> 2a$ and $h >> 2b$, respectively, in order to avoid the effect of the plate boundary and to assure that the applied tension stress is remotely located from the elliptical hole surfaces. The resultant circumferential stress component for an elliptical hole (Fig. 2.3) is [3]

$$\sigma_\xi = \sigma e^{2\xi_o}\left[\frac{\left(1 + e^{-2\xi_o}\right)\sinh(2\xi_o)}{\cosh(2\xi_o) - \cos(2\psi)} - 1\right] \tag{2.14}$$

Using Eq. (2.12) yields

$$\tanh\xi_o = \frac{b}{a} \tag{a}$$

The maximum local stress equation at the tip of the elliptic hole (point a in Fig. 2.3 where $\psi = 0$ and $\cos(2\psi) = 1$) can be derived by manipulating Eq. (2.14) along with the following hyperbolic relationships

$$e^{2\xi_o} = \sinh(2\xi_o) + \cosh(2\xi_o) \tag{b}$$

$$e^{-2\xi_o} = \sinh(2\xi_o) - \cosh(2\xi_o) \tag{c}$$

$$2\sinh^2(\xi_o) = \cosh(2\xi_o) - 1 \tag{d}$$

$$\cosh^2(2\xi_o) = \sinh^2(\xi_o) + \cosh^2(\xi_o) \tag{e}$$

$$\sinh(2\xi_o) = 2\sinh(\xi_o)\cosh(\xi_o) \tag{f}$$

The resultant equation is

$$\sigma_{\xi-\max} = \sigma_{\max} = \sigma_y = \sigma\left[1 + \frac{2\cosh(\xi_o)}{\sinh(\xi_o)}\right] \tag{2.15}$$

Combining Eqs. (2.12) and (2.15) yields the well-known expression in the literature for the maximum local stress in a plate containing an elliptic hole. Thus,

$$\sigma_{\max} = \sigma\left(1 + \frac{2a}{b}\right) \tag{2.16}$$

The reader should consult other references [10–12] in the field of theory of elasticity applied to components containing notches and specific stress concentration factors. With respect to Eq. (2.16), the expression $(1 + 2a/b)$ is known as the theoretical stress concentration factor for an ellipse. Thus,

$$K_t = 1 + \frac{2a}{b} = \frac{\sigma_{\max}}{\sigma} \tag{2.17}$$

Combining Eqs. (2.13) and (2.16) yields the axial stress equation as

$$\sigma_{\max} = \left(1 + 2\sqrt{\frac{a}{\rho}}\right)\sigma \tag{2.18}$$

For a sharp crack, $a >> \rho$, $\sqrt{a/\rho} >> 1$ and Eq. (2.18) becomes

$$\sigma_{\max} = \left(2\sqrt{\frac{a}{\rho}}\right)\sigma \tag{2.19}$$

Thus, the theoretical stress concentration factor becomes

$$K_t = 2\sqrt{\frac{a}{\rho}} = \frac{\sigma_{\max}}{\sigma} \tag{2.20}$$

In fact, the use of the stress concentration approach is meaningless for characterizing the behavior of sharp cracks because the theoretical axial stress concentration factor is $K_t \to \infty$ as $\rho \to 0$. Therefore, the elliptic hole becomes a sharp crack, and the stress intensity factor K_I is the most useful approach for analyzing structural and machine components containing sharp cracks.

Here, σ is the nominal stress or the driving force. If $a = b$, then Eq. (2.16) gives $K_t = 3$ and $\sigma_{\max} = 3\sigma$ for a circular hole. On the other hand, if $b \to 0$

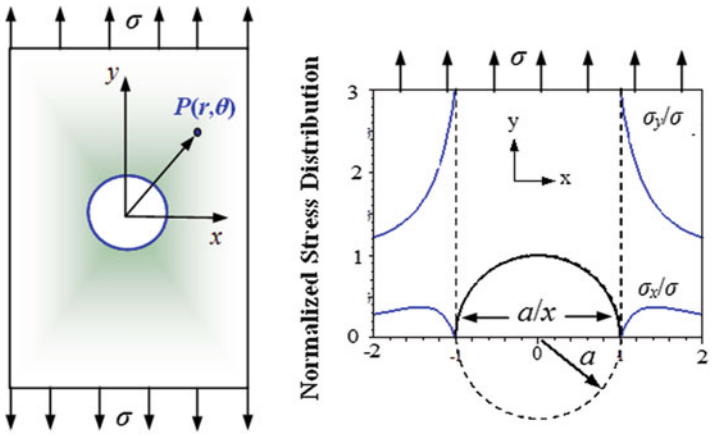

Fig. 2.4 Normalized axial and transverse stresses along the x-axis near a circular hole in a thin plate under tension loading

and $\rho \rightarrow 0$, then a sharp crack is formed and $\sigma_{\max} \rightarrow \infty$, which is singular and meaningless. In addition, K_t is used to analyze the stress field at a point in the vicinity of a notch having a radius $\rho >> 0$. However, if a crack is formed having $\rho \simeq 0$ at a microscopic level, the stress field at the crack tip is defined in terms of the stress intensity factor (K_I) instead of the stress concentration factor (K_t). In fact, microstructural discontinuities and geometrical discontinuities, such as notches, holes, grooves, and the like, are sources of crack initiation when the stress concentration factor is sufficiently high.

Symmetric Circular Hole in an Infinite Plate Figure 2.4 shows the distribution of the axial and transverse normalized stresses along the x-axis near a circular hole in a wide, thin, and infinite plate loaded in tension.

Consider an infinite isotropic plate containing a circular hole as shown in Fig. 2.4. It is desirable to determine the elastic stresses in rectangular and polar coordinates when the plate is remotely loaded in tension.

The detailed analytical procedure for deriving the generalized stress equations in polar coordinates, based on the method of superposition, can be found in a book written by Dally and Riley [1]. Thus, these equations evaluated at point $P(r, \theta)$ are

$$\begin{aligned}
\sigma_r &= \frac{\sigma}{2}\left\{\left(1-\frac{a^2}{r^2}\right)\left[1+\left(\frac{3a^2}{r^2}-1\right)\cos 2\theta\right]\right\} \\
\sigma_\theta &= \frac{\sigma}{2}\left[\left(1+\frac{a^2}{r^2}\right)+\left(1+\frac{3a^4}{r^4}\right)\cos 2\theta\right] \\
\tau_{r\theta} &= \frac{\sigma}{2}\left[\left(1+\frac{3a}{r^2}\right)\left(1-\frac{a^2}{r^2}\right)\sin 2\theta\right]
\end{aligned} \tag{2.21}$$

Letting $\theta = 0$ and $r = x$ in Eq. (2.21) yields the stress distribution along the x-axis at point $P(x, 0)$ in Fig. 2.4, where $\sigma_r = \sigma_x$, $\sigma_\theta = \sigma_{yy}$ and $\tau_{r\theta} = \tau_{xy} = 0$. Thus, Eq. (2.21) becomes [1, 12]

$$\begin{aligned} \frac{\sigma_x}{\sigma} &= \frac{3}{2}\left(\frac{a}{x}\right)^2 - \frac{3}{2}\left(\frac{a}{x}\right)^4 \\ \frac{\sigma_y}{\sigma} &= 1 + \frac{1}{2}\left(\frac{a}{x}\right)^2 + \frac{3}{2}\left(\frac{a}{x}\right)^4 \\ \frac{\tau_{xy}}{\sigma} &= 0 \end{aligned} \tag{2.22}$$

2.4 Griffith Crack Theory

The development of linear-elastic fracture mechanics (LEFM) started with Griffith work on glass [4]. Fundamentally, the Griffith theory considers the energy changes associated with incremental crack growth. He used an energy balance approach to predict the fracture stress of glass and noted in 1921 that when a stressed plate of an elastic material containing cracks, the potential energy per unit thickness (ΔU) decreased and the surface energy per unit thickness (U_s) increased during crack growth. Then, the total potential energy of the stressed solid body is related to the release of stored energy and the work done by the external loads. The "surface energy" arises from a nonequilibrium configuration of the nearest neighbor atoms at any surface in a solid [13–15].

Consider a large or an infinite brittle plate containing one center through-thickness crack of length $2a$ with two crack tips as depicted in Fig. 2.5. When the plate is subjected to a remote and uniform tensile load perpendicular to the crack plane along the x-axis, the stored elastic strain energy is released within a cylindrical volume of material of length B.

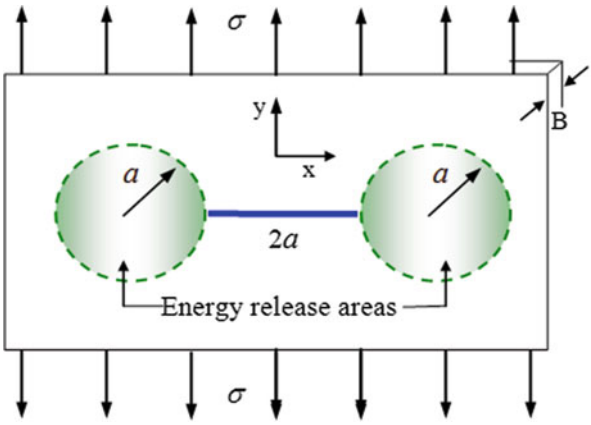

Fig. 2.5 A large plate containing one through-thickness central crack. Also shown are two idealized energy release areas ahead of the crack tips

When the elastic or brittle solid body (specimen) is remotely loaded from the crack faces, the product of the released elastic strain energy density ($\int \sigma d\epsilon$) and the cylindrical volume element ($2\pi a^2 B$) about the crack (Fig. 2.5), where this energy is released, yields the elastic strain energy as

$$W_e = -2\left(\pi a^2 B\right)\int \sigma d\epsilon = -2\left(\pi a^2 B\right)\int E'\epsilon d\epsilon \tag{2.23}$$

$$W_e = -2\left(\pi a^2 B\right)\left(\frac{E'\epsilon^2}{2}\right) = -\left(\pi a^2 B\right)\left(\frac{\sigma^2}{E'}\right) \tag{2.24}$$

where $\sigma = E'\epsilon =$ Hooke's law
$E' = E$ for plane stress
$E' = E/\left(1 - v^2\right)$ for plane-strain conditions
$E =$ Modulus of elasticity (MPa)
$\epsilon =$ Elastic strain
$\sigma =$ Applied remote stress (MPa)
$a =$ One-half crack length (mm)
$v =$ Poisson's ratio
$4aB = 2(2aB) =$ Total surface crack area (mm^2)
$B =$ Thickness (mm)

Denote that the factor E' is introduced in Eq. (2.23) for controlling either plane stress or plane-strain condition. In addition, Eq. (2.24) can also be derived by inserting the Inglis displacement equation (μ_y) in the y-direction [3] into the following expression:

$$W_e = -4B\int_o^a \frac{1}{2}\sigma\mu_y dx = -4B\int_o^a \frac{1}{2}\sigma\left(\frac{2\sigma}{E'}\sqrt{a^2 - x^2}\right)dx \tag{a}$$

$$W_e = -\left(\frac{4B\sigma^2}{E'}\right)\int_o^a \sqrt{a^2 - x^2}dx = -\left(\frac{4B\sigma^2}{E'}\right)\left(\frac{\pi a^2}{4}\right) \tag{b}$$

$$W_e = -\left(\pi a^2 B\right)\left(\frac{\sigma^2}{E'}\right) \tag{2.25}$$

Now, the elastic surface energy for creating new crack surfaces during crack growth (from two crack tips) is [4]

$$W_s = 2\left(2aB\gamma_s\right) \tag{2.26}$$

where $\gamma_s =$ Specific surface energy for atomic bond breakage (J/mm^2)

For an elastically stressed solid body, Griffith energy balance takes into account the decrease in potential energy (due to the release of stored elastic energy and the work done by external loads) and the increase in surface energy resulting from the growing crack, which creates new surfaces. For the energy balance, the total elastic

energy of the system, referred to as the total potential energy, takes the mathematical form

$$W = W_s + W_e = 2\,(2aB\gamma_s) - \left(\pi a^2 B\right)\left(\frac{\sigma^2}{E'}\right) \tag{2.27}$$

For convenience, divide Eq. (2.27) by the thickness B to get the total potential energy per unit thickness as

$$U = U_s + U_e \tag{2.28}$$

$$U = 2\,(2a\gamma_s) - \frac{\pi a^2\sigma^2}{E'} \tag{2.29}$$

where U_s = Elastic surface energy per unit thickness (J/mm)
U_e = Released elastic energy per unit thickness (J/mm)

Thus, the Griffith's energy criterion for crack growth is $U_e \geq U_s$ when $dU/da = 0$. Then, the energy balance gives $4a\gamma_s E' = \beta\pi a^2\sigma^2$, from which the applied stress (σ), the crack length (a) or the strain energy release rate (G_I) for brittle solid materials are easily derivable. They are, respectively,

$$\sigma = \sqrt{\frac{(2\gamma_s)E'}{\pi a}} \tag{2.30}$$

$$a = \frac{(2\gamma_s)E'}{\pi\sigma^2} \tag{2.31}$$

$$G_I = 2\gamma_s = \frac{\pi a\sigma^2}{E'} \tag{2.32}$$

At fracture, Eqs. (2.30) through (2.32) give the critical entities. Rearranging Eq. (2.32) yields the elastic stress intensity factor

$$\sigma\sqrt{\pi a} = \sqrt{(2\gamma_s)E'} = \sqrt{G_I E'} \tag{2.33}$$

$$K_I = \sigma\sqrt{\pi a} \tag{2.34}$$

The parameter K_I is called the stress intensity factor which is the crack driving force, and its critical value is a material property known as fracture toughness, which, in turn, is the resistance force to crack extension [16]. The interpretation of Eq. (2.34) suggests that crack extension in brittle solids is completely governed by the critical value of the stress intensity factor.

Griffith observed that $\sigma_f\sqrt{a_c}$ was nearly a constant for six (6) cracked circular glass tubes under plane stress condition, Table III in ref. [4]. The average value is

$$\sigma_f\sqrt{a_c} = 0.2378 \pm 0.0062\,\text{ksi}\sqrt{\text{in}} \tag{a}$$

For convenience, using Eq. (2.34) yields the plane-strain fracture toughness

$$K_{IC} = \sigma_f \sqrt{\pi a_c} \simeq 0.42 \pm 0.01 \,\text{ksi}\sqrt{\text{in}} \tag{b}$$
$$K_{IC} = 0.46 \pm 0.01 \,\text{MPa}\sqrt{\text{m}}$$

In addition, taking the second derivative of Eq. (2.29) with respect to the crack length yields

$$\frac{d^2(U)}{da^2} = -\frac{2\pi\sigma^2 B}{E'} \tag{2.35}$$

Denote that $d^2U/da^2 < 0$ represents an unstable system. Consequently, the crack will always grow [15]. Fundamentally, linear-elastic fracture mechanics requires a stress analysis approach to predict nonphysical or conceptual infinite local stresses ($\sigma_{ij} \rightarrow \infty$) at a crack tip despite that yielding occurs, to an extent, in most engineering brittle solids. Glass and the pure brittle materials are an exception. The yielding process truncates the local stresses, specifically the stress perpendicular (σ_y) to the crack plane. Eventually, the maximum applied stress is a critical (σ_c) or fracture stress (σ_f) that causes fracture of the solid is less than the yield strength (σ_{ys}) of the solid body due to the existence of cracks or defects.

Example 2.1. *A large and wide brittle plate containing a single-edge crack (a) fractures at a tensile stress of* 4 *MPa. The critical strain energy release rate* (G_c) *and the modulus of elasticity (E) are* $4\,J/m^2$ *and* 65,000 *MPa, respectively. Assume plane stress condition and include the thickness* $B = 3$ *mm in all calculations.* **(a)** *Plot the theoretical total surface energy* (U_s)*, the released strain energy* (U_e)*, and the total potential energy change (W). Interpret the energy profiles. Determine* **(b)** *the critical crack length and* **(c)** *the maximum potential energy change* ($W_{\max}$)*;* **(d)** *will the crack grow unstably?* **(e)** *What is the critical stress intensity factor for this brittle plate?*

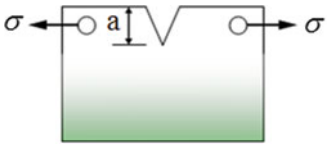

Solution. *Given data:*
$\sigma = 4\,\text{MPa}$*;* $E' = E = 65{,}000\,\text{MPa}$ *for plane stress condition*
$G_c = 4\,\text{J/m}^2 = 4 \times 10^{-6}\,\text{J/mm}^2$
$\gamma_s = G_c/2 = 2\,\text{J/m}^2 = 2 \times 10^{-6}\,\text{J/mm}^2$

(a) *For single-edge crack with one crack tip, Eq. (2.27) is divided by* 2*. Thus, the surface energy becomes*

$$W_s = 2aB\gamma_s = (2)\left(3\times10^{-3}\ \text{m}\right)\left(2\ \text{J/m}^2\right)a = \left(12\times10^{-3}\ \text{J/m}\right)a$$

$$W_s = \left(12\times10^{-6}\ \text{J/mm}\right)a$$

On the other hand, the released strain energy is also divided by 2 *so that*

$$W_e = -\left(\pi a^2 B\right)\left(\frac{\sigma^2}{2E}\right)$$

$$W_e = -\frac{(\pi)\left(3\times10^{-3}\ \text{m}\right)(4\ \text{MPa})^2\,a^2}{(2)\,(65000\ \text{MPa})} = -\left(1.16\times10^{-6}\ \text{MPa m}\right)a^2$$

$$W_e = -\left(1.16\ \text{Pa m}\right)a^2 = \left(1.16\ \text{J/m}^2\right)a^2$$

$$W_e = -\left(1.16\times10^{-6}\ \text{J/mm}^2\right)a^2$$

Thus, the potential energy change becomes

$$W = W_s + W_e$$

$$W = \left(12\times10^{-6}\ \text{J/mm}\right)a - \left(1.16\times10^{-6}\ \text{J/mm}^2\right)a^2$$

The energy profiles are given below. The total potential energy associated with crack growth is simply the sum of the surface energy and the released strain energy. The former energy is needed for creating new crack surfaces by allowing the breakage of atomic bonds. The latter energy is negative because it is released during crack growth and it is needed for unloading the regions near the crack flanks.

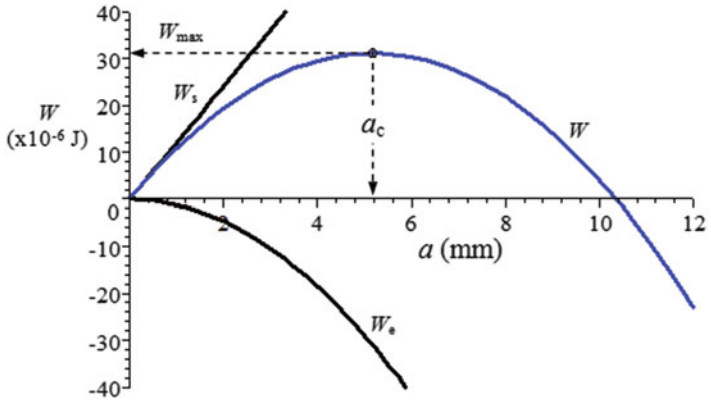

Moreover, stable crack growth occurs when $W < W_{\max}$, but $W > 0$. At the maximum potential energy, the crack length reaches a critical value $a = a_c$ and the slope becomes $dW/da = 0$. Beyond this critical state, the potential energy change decreases very significantly because crack growth continues to occur at a very high velocity causing catastrophic failure.

(b) *The critical crack length can be determined by letting the first-order derivative of the total potential energy equals to zero. Thus,*

$$W = \left(12 \times 10^{-6}\ \text{J/mm}\right) a - \left(1.16 \times 10^{-6}\ \text{J/mm}^2\right) a^2$$

$$\left.\frac{dW}{da}\right|_{a=a_c} = \left(12 \times 10^{-6}\ \text{J/mm}\right) - \left(2.32 \times 10^{-6}\ \text{J/mm}^2\right) a_c = 0$$

$$a_c = \frac{12 \times 10^{-6}}{2.32 \times 10^{-6}} = 5.17\ \text{mm} = 0.20\ \text{in}$$

Therefore, $a_c = 5.17\,mm$ is not a very large crack, but it is the maximum allowable crack length in the system. If a similar structure is to be put in service, then a crack detection technique has to be implemented in order to avoid fracture when $a = a_c$.

(c) *The maximum potential energy is*

$$W_{\max} = \left(12 \times 10^{-6}\ \text{J/mm}\right) a_c - \left(1.16 \times 10^{-6}\ \text{J/mm}^2\right) a_c^2$$

$$W_{\max} = \left(12 \times 10^{-6}\ \text{J/mm}\right) (5.17\ \text{mm}) - \left(1.16 \times 10^{-6}\ \text{J/mm}^2\right) (5.17\ \text{mm})^2$$

$$W_{\max} = 31.03 \times 10^{-6}\ \text{J}$$

Thus, the point $(a_c, W_{\max}) = \left(5.17\ mm,\ 31.03 \times 10^{-6}\ J\right)$ is plotted on the figure above. At this critical point, the derivative of the total potential energy change is $d(W)/da = 0$ and $W = W_{\max}$ at $a = a_c$.

(d) *From part* **(a)**,

$$W = \left(12 \times 10^{-6}\ \text{J/mm}\right) a - \left(1.16 \times 10^{-6}\ \text{J/mm}^2\right) a^2$$

$$\frac{dW}{da} = \left(12 \times 10^{-6}\ \text{J/mm}\right) - \left(2.32 \times 10^{-6}\ \text{J/mm}^2\right) a$$

$$\frac{d^2W}{da^2} = -2.32 \times 10^{-6}\ \text{J/mm}^2$$

Therefore, the crack will grow unstable because $d^2W/da^2 < 0$.

(e) *The critical stress intensity factor or the plane stress fracture toughness for the brittle plate is determined by using Eq. (2.34). Thus,*

$$K_C = \sigma\sqrt{\pi a_c}$$
$$K_C = (4\ \text{MPa})\sqrt{\pi\,(5.17 \times 10^{-3}\ \text{m})}$$
$$K_C = 0.51\ \text{MPa}\sqrt{\text{m}}$$

In addition, combining Eqs. (2.30) and (2.34) along $\beta = 1$, $K_I = K_C$ *and* $a = a_c$ *gives*

$$K_C = \sqrt{2\gamma_s E} = \sqrt{2\left(2\ \text{J/m}^2\right)(65000 \times 10^6\ \text{Pa})}$$
$$K_C = \sqrt{2\,(2\ \text{Pa m})\,(65000 \times 10^6\ \text{Pa})}$$
$$K_C = 5.1 \times 10^5\ \text{Pa}\sqrt{\text{m}}$$
$$K_C = 0.51\ \text{MPa}\sqrt{\text{m}}$$

Also, combining Eqs. (2.29) and (2.34) yields

$$K_C = \sqrt{\frac{2E}{a_c B}\left(2a_c B\gamma_s - W_{\max}\right)} = 0.51\ \text{MPa}\sqrt{\text{m}}$$

Therefore, the above mathematical equations give the same low result for K_C*, which, in turn, indicates that the material is brittle and it is an important property of the material for design applications. In fact,* K_C *is the plane stress fracture toughness that defines the material resistance to brittle fracture when the crack length reaches a critical value* a_c*. Furthermore, a low* K_C *value implies that the material absorbs a small quantity of strain energy prior fracture. This indicates that the materials is elastic or brittle. Hence, brittle materials can be used in specific engineering applications.*

On the other hand, a large K_C *value specifies a larger consumption of strain energy and the material fractures in a tearing-like mode. This, then, defines a ductile material, which may have significant applications in industrial structures.*

2.5 Strain Energy Release Rate

It is well known that plastic deformation occurs in engineering metal, alloys, and some polymers. Due to this fact, Irwin [2] and Orowan [17] modified Griffith's elastic surface energy expression, Eq. (2.32), by adding a plastic deformation energy or plastic strain work γ_p in the fracture process. For tension loading, the total elastic-

plastic strain energy is known as the strain energy release rate G_I, which is the energy per unit crack surface area available for infinitesimal crack extension [16]. Thus,

$$G_I = 2\left(\gamma_s + \gamma_p\right) \tag{2.36}$$

$$G_I = \frac{\pi a \sigma^2}{E'} \tag{2.37}$$

Here, $E' = E/\beta$. Rearranging Eq. (2.37) gives the stress equation as

$$\sigma = \sqrt{\frac{E' G_I}{\pi a}} \tag{2.38}$$

Combining Eqs. (2.34) and (2.37) yields

$$G_I = \frac{K_I^2}{E'} \tag{2.39}$$

This is one of the most important relations in the field of linear fracture mechanics. Hence, Eq. (2.39) suggests that G_I represents the material's resistance (R) to crack extension, and it is known as the crack driving force. On the other hand, K_I is the intensity of the stress field at the crack tip.

The condition of Eq. (2.39) implies that $G_I = R$ before relatively slow crack growth occurs. However, rapid crack growth (propagation) takes place when $G_I \rightarrow G_{IC}$, which is the critical strain energy release rate known as the crack driving force or fracture toughness of a material under tension loading. Consequently, the fracture criterion by G_{IC} establishes crack propagation when $G_I \geq G_{IC}$. In this case, the critical stress or fracture stress σ_c and the critical crack driving force G_{IC} can be predicted using Eq. (2.39) when the crack is unstable. Hence, the critical or fracture stress is defined as

$$\sigma_f = \sigma_c = \sqrt{\frac{E' G_{IC}}{\pi a}} \tag{2.40}$$

Griffith assumed that the crack resistance R consisted of surface energy only for brittle materials. This implies that $R = 2\gamma_s$, but most engineering materials undergo, to an extent, plastic deformation so that $R = 2\left(\gamma_s + \gamma_p\right)$. Figure 2.6 shows a plastic zone at the crack tip representing plasticity or localized yielding, induced by an external nominal stress. This implies that the energy γ_p is manifested due to this small plastic zone in the vicinity of the crack tip.

It is clear that the internal stresses on an element of an elastic-plastic boundary are induced by plasticity and are temperature-dependent tensors. The stress in front of the crack tip or within the plastic zone exceeds the local microscopic yield stress,

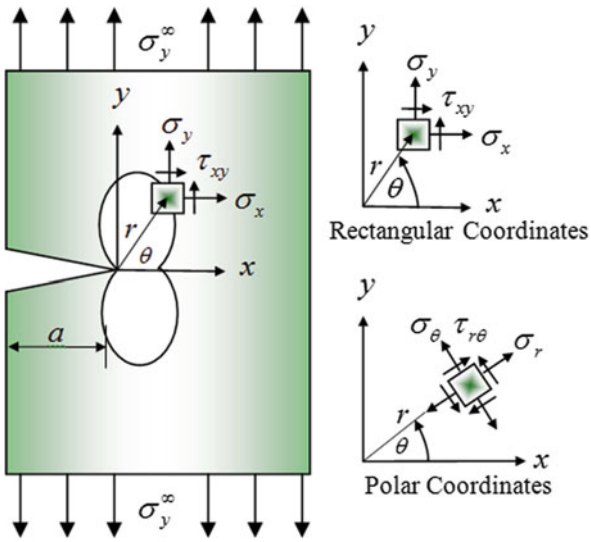

Fig. 2.6 Single-edge crack configuration showing the plastic zone and stresses at the crack tip is rectangular and polar coordinates

which may be defined as the theoretical or cohesive stress for breaking atomic bonds. If microscopic plasticity through activated slip systems does not occur, as in glasses, then a linear-elastic fracture is achieved as the controlling fracture process. In essence, the fracture process is associated with plasticity at a microscopic level.

If large plasticity occurs at the crack tip, then the crack blunts and its radius of curvature increase. This plastic deformation process is strongly dependent on the temperature and microstructure. Regardless of the shape of the plastic zone, the irreversible crack tip plasticity is an indication of a local strain hardening process during which slip systems are activated and dislocations pile up and dislocation interaction occurs.

Example 2.2. *This worked example illustrates the application of fracture mechanics to determine the behavior of a cracked solid body subjected to a static stress. A hypothetical (*1-*m*) × (100-*mm*) × (3-*mm*) sheet of glass containing a 0.4-mm-long central crack (slit) is loaded in tension by a hanging person having a mass of* 80 *Kg.* **(a)** *Calculate* K_I *and* G_I *at fracture.* **(b)** *Determine whether or not the glass sheet will fracture. The fracture toughness and the modulus of elasticity of glass are* $K_{IC} = 0.80\,MPa\sqrt{m}$ *and* $E = 60\,GPa$*, respectively. Calculate* **(c)** *the critical crack length (*a_c*) which is the maximum allowable crack size before fast fracture occurs,* **(d)** *the fracture or critical stress,* **(e)** *the reduction in strength if the crack-free (sound) fracture stress is* 165 *MPa, and* **(f)** *the maximum allowable mass (*m_c*). Assume a Poisson's ratio of* 0.3 *and plane stress conditions because the plate is very thin.*

Solution.

(a) *The applied mass has to be converted to a load, which in turn is divided by the cross-sectional area of the plate as if the crack is not present. Also, the specimen configuration is given below.*

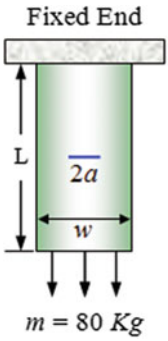

The applied stress, the stress intensity factor, and the strain energy release rate are, respectively,

$$\sigma = P/A_o = \frac{(80\text{ Kg})\left(9.81\text{ m/s}^2\right)}{(100\times10^{-3}\text{ m})\,(3\times10^{-3}\text{ m})} = 262\text{ MPa}$$

$$K_I = \sigma\sqrt{\pi a} = (262\text{ MPa})\sqrt{\pi\,(0.2\times10^{-3}\text{ m})} = 0.07\text{ MPa}\sqrt{\text{m}}$$

$$G_I = \frac{K_I^2}{E} = \frac{\left(0.07\text{ MPa}\sqrt{\text{m}}\right)^2}{11\times10^3\text{ MPa}} = 4.45\times10^{-7}\text{ MPa} = 0.445\text{ J/m}^2$$

(b) *The sheet of glass will not fracture because* $K_I < K_{IC}$.

(c) *Let* $K_I < K_{IC}$ *and* $a < a_c$ *in Eq. (2.34) so that the maximum allowable crack length under the loading condition becomes*

$$K_{IC} = \sigma\sqrt{\pi a_c}$$

$$a_c = \frac{1}{\pi}\left(\frac{K_{IC}}{\sigma}\right)^2 = \frac{1}{\pi}\left(\frac{0.80\text{ MPa}\sqrt{\text{m}}}{262\text{ MPa}}\right)^2 = 29.68\text{ mm}$$

(d) *From Eq. (2.39),* $G_I = G_C$

$$G_C = \frac{K_{IC}^2}{E} = \frac{\left(0.80\text{ MPa}\sqrt{\text{m}}\right)^2}{60\times10^3\text{ MPa}}$$

$$G_C = 1.067\times10^{-5}\text{ MPa}\cdot\text{m} = 10.67\text{ J/m}^2$$

From Eq. (2.38), the applied stress at fracture is just the critical stress; that is, $\sigma = \sigma_c$

$$\sigma_c = \sqrt{\frac{EG_C}{\pi a}} = \sqrt{\frac{(60 \times 10^3 \text{ MPa})\,(9.71 \times 10^{-6} \text{ MPa} \cdot \text{m})}{\pi\,(0.2 \times 10^{-3} \text{ m})}}$$

$$\sigma_c = 31.92 \text{ MPa}$$

The critical stress for fracture can also be calculated using the critical stress intensity factor K_{IC}*. Thus,*

$$\sigma_c = \frac{K_{IC}}{\sqrt{\pi a_c}} = \frac{0.80 \text{ MPa}\sqrt{\text{m}}}{\sqrt{\pi\,(0.2 \times 10^{-3} \text{ m})}}$$

$$\sigma_c = 31.92 \text{ MPa}$$

(e) *The reduction in strength due to a small crack is*

$$\frac{165 - 31.92}{165} \times 100\,\% = 80.65\,\%$$

This particular result indicates how critical is the presence of small defects in solid bodies.

(f) *The maximum allowable or critical mass can be determined using the following critical stress equation*

$$\sigma_c = \frac{m_c g}{A_o}$$

$$m_c = \frac{A_o \sigma_c}{g}$$

Hence, the critical mass is

$$m_c = \frac{A_o \sigma_c}{g} = \frac{\left(100 \times 10^{-3} \text{ m}\right)\left(3 \times 10^{-3} \text{ m}\right)\left(31.92 \times 10^6 \text{ N/m}^2\right)}{\left(9.81 \text{ m/s}^2\right)}$$

$$m_c = 976.15 \text{ Kg}$$

The critical mass can also be calculated using the critical stress intensity factor (plane-strain fracture toughness) as follows:

$$m_c = \frac{A_o K_{IC}}{g\sqrt{\pi a_c}} = \frac{\left(100 \times 10^{-3} \text{ m}\right)\left(3 \times 10^{-3} \text{ m}\right)\left(0.80 \times 10^6 \text{ Pa}\sqrt{\text{m}}\right)}{\left(9.81 \text{ m/s}^2\right)\sqrt{\pi\,(0.2 \times 10^{-3} \text{ m})}}$$

$$m_c = 976.01 \text{ Kg}$$

The slight difference in the critical mass is due to the truncation error involved in all calculations.

It is obvious, in general, that the existence of different crack configurations is quite detrimental or fatal to structures under a loading mode. The current example is very simple, but exhibits an important analysis in determining the critical crack length a structural component can tolerate before crack propagation toward fracture takes place. This example also reflects the importance of fracture mechanics in designing applications to assure structural integrity during a design lifetime.

2.6 Grain-Boundary Strengthening

This technique is used to enhance the strength and the fracture toughness of polycrystalline materials, such as low-carbon steels. The classical Hall–Petch model [18, 19] is commonly used to predict the mechanical behavior of polycrystalline materials since it correlates the yield strength with the grain size (d) to an extent. The Hall–Petch model is based on a planar dislocation pileup mechanism in an infinite and homogeneous medium as schematically shown in Fig. 2.7. The dislocation pileup is modeled as a series of edge dislocations ($\perp$) emanating from a source toward the grain boundary on a particular slip plane.

The mathematical form of the Hall–Petch model for the yield strength is

$$\sigma_{ys} = \sigma_o + k_y d^{-1/2} \tag{2.41}$$

where σ_o = Lattice friction stress (MPa)

k_y = Dislocation locking term (MPa$\sqrt{\text{m}}$)

Briefly, if a dislocation source is activated, then it causes dislocation motion to occur toward the grain boundary, which is the obstacle suitable for dislocation pileup. Thus, dislocation motion encounters the lattice friction stress σ_o as dislocations move on a slip plane toward a grain boundary. This dislocation-based model assumes that dislocation motion is the primary mechanism for plastic flow in crystalline materials and it is the basis for the Hall–Petch equation. In addition,

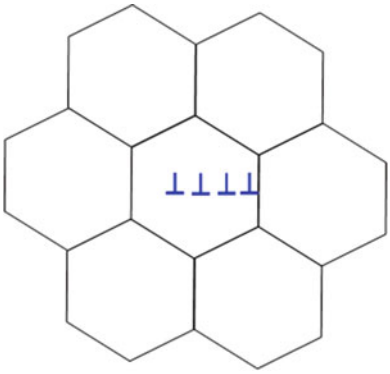

Fig. 2.7 Edge dislocation pileup model

the pileup causes a stress concentration at the grain boundary, which eventually fractures when the local stress (shear stress) reaches a critical value. Therefore, other dislocation sources are generated. This is a possible mechanism for explaining the yielding phenomenon from one grain to the next. However, the grain size dictates the size of dislocation pileup, the distance dislocations must travel, and the dislocation density associated with yielding. This implies that the finer the grains, the higher the yield strength.

If a suitable volume of hard particles exists in a fine-grain material, the yield stress is enhanced further since three possible strengthening mechanisms are present, that is, solution strengthening, fine-grain strengthening, and particle (dispersion) strengthening. If these three strengthening mechanisms are activated, then the Hall–Petch model is not a suitable model for explaining the mechanical behavior of polycrystalline materials. This suitable explanation is vital in understanding that the grain size plays a major role in determining material properties such as the yield strength and fracture toughness.

Further, the Hall–Petch model can also be used to correlate hardness and grain size as indicated below:

$$H = H_o + k_h d^{-1/2} \tag{2.42}$$

Here, H_o and k_h are constants which are determined through a curve fitting procedure. Nonetheless, the physical foundation of this empirical equation is assumed to be associated with dislocation pileup within grains.

The understanding of the mechanical behavior of polycrystalline materials from nano- to microscales is very important scientifically and technologically because the grain size (d) plays a critical role in designing materials having desired mechanical properties.

The crossover from normal to inverse Hall–Petch model is depicted in Fig. 2.8 [20, 21]. The inverse Hall–Petch model is found in the new generation of advanced materials with nanostructures or nano-grains [7, 22–25].

Figure 2.8 illustrates three different regions: (1) the micro-grain region in which the conventional Hall–Petch can be used, (2) the transitional region where the maximum hardness corresponds to a critical grain size (d_c) and beyond this point the Hall–Petch model is reversed having a negative slope, and (3) the nano-grain region in which the grains are very small leading to large values of $d^{-1/2}$, which in turn cause a decrease in hardness. The specific hardness or yield strength profile for materials having very small grains at a nanoscale depends on the inherent peculiarities of the nanostructures, which have large grain-boundary areas. Currently, excellent publications on the reverse Hall–Petch model are available in the literature; however, this is a subject of so much controversy [21].

Furthermore, letting the crack length be in the order of the average grain size ($d = a$), it can be shown that both yield strength (σ_{ys}) and the critical strain energy release rate (G_{IC}) known as fracture toughness depend on the grain size. Using the

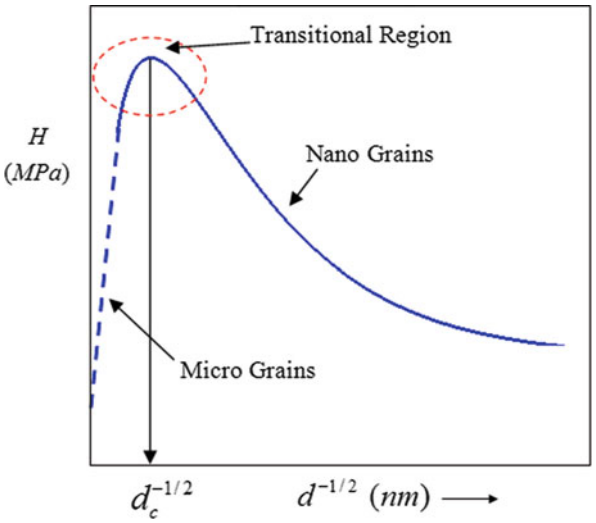

Fig. 2.8 Schematic hardness profile showing the normal to inverse Hall–Petch model

Hall–Petch equation, Eq. (2.41), for σ_{ys} and Eq. (2.40) for σ_f, it is clear that these stress entities depend on the grain size. Hence,

$$\sigma_f = \left(\frac{E'G_{IC}}{\pi}\right)^{1/2} d^{-1/2} = k_f d^{-1/2} \tag{2.43}$$

where k_f = Constant (MPa$\sqrt{\text{m}}$)

Denote that Eqs. (2.41) and (2.43) predict that $\sigma_{ys} = f(d)$ and $\sigma_f = f(d)$. The slopes of these functions, k_y and k_f, respectively, have the same units, and they may be assumed to be related to fracture toughness. The slope k_y is referred to as the dislocation locking term that restricts yielding from a grain to the adjacent one. Mathematically, the analysis of Eq. (2.40) through (2.43) for materials having temperature and grain size dependency indicate that $\sigma_{ys} \to \infty$, $\sigma_f \to \infty$ and $H \to \infty$ as $d \to 0$. Physically, these entities have limited values and $\sigma_f \geq \sigma_{ys}$ due to the inherent friction stress (σ_o) at a temperature T_1. At a temperature $T_2 > T_1$, σ_{ys} decreases since σ_o and k_y also decrease, and G_{IC} increases and, therefore, σ_f must decrease.

One can observe that $\sigma_{ys} \to \sigma_o$ for $d^{-1/2} = 0$, which means that σ_o is regarded as the yield stress of a single crystal. However, $\sigma_{ys} \to \sigma_o$ and $\sigma_f \to \sigma_o$ as $d \to \infty$ is an unrealistic case. Therefore, grain size refinement is a useful strengthening mechanism for increasing both σ_{ys} and σ_f.

Finally, if one combines Eqs. (2.34) and (2.42) along with $d = a$, one can determine that the K_I is inversely proportional to hardness. Thus,

$$K_I = \frac{k_h \sigma \sqrt{\pi}}{H - H_o} \approx \frac{k_h \sigma \sqrt{\pi}}{H} \tag{2.44}$$

Here, it can be assumed that k_h is a correction factor and $H >> H_o$.

2.7 Problems

2.1. Show that the applied stress is $\sigma \to 0$ when the crack tip radius is $\rho \to 0$. Explain.

2.2. In order for crack propagation to take place, the strain energy is defined by the following inequality $U(a) - U(a + \Delta a) \geq 2\Delta a\gamma$, where Δa is the crack extension and γ is the surface energy. Show that the crack driving force or the strain energy release rate at instability is defined by $G \geq dU(a)/da$.

2.3. One (1-mm) × (15-mm) × 100-mm steel strap has a 3-mm-long central crack. This strap is loaded in tension to failure. Assume that the steel is brittle having the following properties: $E = 207\,\text{GPa}$, $\sigma_{ys} = 1500\,\text{MPa}$, and $K_{IC} = 70\,\text{MPa}\sqrt{\text{m}}$. Determine (a) the critical stress and (b) the critical strain energy release rate.

2.4. Suppose that a structure made of plates has one cracked plate. If the crack reaches a critical size, will the plate fracture or the entire structure collapse? Explain.

2.5. What is crack instability according to Griffith criterion?

2.6. Assume that a quenched $1.2\%C$-steel plate has a penny-shaped crack. Will the Griffith theory be applicable to this plate?

2.7. Will the Irwin theory be valid for a changing plastic zone size during crack growth?

2.8. What are the major roles of the surface energy and the stored elastic energy during crack growth?

2.9. What does happen to the elastic energy during crack growth?

2.10. What does $dU/da = 0$ mean?

2.11. Derive Eq. (2.29) starting with Eq. (2.20).

References

1. J.W. Dally, W.F. Riley, *Experimental Stress Analysis*, 3rd edn. (McGraw-Hill, New York, 1991)
2. G.R. Irwin, Fracture I, in *Handbuch der Physik VI*, ed. by S. Flugge (Springer, New York, 1958) 558–590
3. C.E. Inglis, Stresses in a plate due to the presence of cracks and sharp corners. Trans. Inst. Nav. Archit. **55**, 219–241 (1913)

4. A.A. Griffith, The phenomena of rupture and flows in solids. Philos. Trans. R. Soc. **221**, 163–198 (1921)
5. H.M. Westergaard, Bearing pressures and cracks. J. Appl. Mech. **G1**, A49–A53 (1939)
6. W.J. McGregor Tegart, *Elements of Mechanical Metallurgy* (Macmillan, New York, 1966)
7. M. Rieth, *Nano-Engineering in Science and Technology : An Introduction to the World of Nano-Design*. Series on the Foundations of Natural Science and Technology, vol. 6 (World Scientific, Singapore, 2003)
8. K. Ashbee, *Fundamental Principles of Fiber Reinforced Composites*, 2nd edn. (CRC Press, West Palm Beach, 1993), pp. 211–218
9. A.P. Boresi, O.M. Sidebottom, *Advanced Mechanics of Materials* (Wiley, New York, 1985), pp. 534–538
10. J.A. Collins, *Failure of Materials in Mechanical Design*: *Analysis, Prediction, Prevention*, 2nd edn. (Wiley, New York, 1993), pp. 422–427
11. S.P. Timoshenko, J.N. Goodier, *Theory of Elasticity*, 3rd edn. (McGraw-Hill, New York, 1970), p. 193
12. H.J. Grover, *Fatigue Aircraft Structures* (NAVIR 01-1A-13 Department of the Navy, Washington, DC, 1966)
13. D. Broek, *Elementary Engineering Fracture Mechanics*, 4th edn. (Kluwer Academic, Boston, 1986)
14. K. Hellan, *Introduction to Fracture Mechanics* (McGraw-Hill, New York, 1984)
15. R.W. Hertzberg, *Deformation and Fracture Mechanics of Engineering Materials*, 3rd edn. (Wiley, New York, 1989)
16. J.M. Barsom, S.T. Rolfe, *Fracture and Fatigue Control in Structures*: *Applications of Fracture Mechanics*, Chap. 2, 3rd edn. (American Society For Testing and Materials, West Conshohocken, PA, 1999)
17. E. Orowan, *Fatigue and Fracture of Metals* (MIT Press, Cambridge, MA, 1950), p. 139
18. E.O. Hall, The deformation and ageing of mild steel: III discussion of results. Proc. Phys. Soc. B Lond. **64**(9), 747–753 (1951)
19. N.J. Petch, The cleavage strength of polycrystals. J. Iron Steel Inst. **174**, 25–28 (1953)
20. T.G. Nieh, J. Wadsworth, Hall-petch relation in nanocrystalline solids. Scr. Mater. **25**, 955–958 (1991)
21. M. Yu Gutkin, I.A. Ovid'ko, C.S. Pande, Theoretical models of plastic deformation processes in nanocrystalline matertials. Rev. Adv. Mater. Sci. **2**(1), 80–102 (2001)
22. A.S. Edelstein, R.C. Cammaratra, *Nanomaterials*: *Synthesis, Properties and Applications* (Taylor & Francis, London, 1998)
23. H.S. Nalwa (ed.), *Handbook of Nanostructured Materials and Nanotechnology*, vol. 1–5 (Academic Press, San Diego, 1999)
24. C.P. Poole Jr., F.J. Owens, *Introduction to Nanotechnology* (Wiley, Hoboken, 2003)
25. G.M. Chow, I.A. Ovid'ko, T. Tsakalakos (eds.), *Nanostructured Films and Coatings*. NATO Science Series (Kluwer Academic, Dordrecht, 2000)

http://www.springer.com/978-3-319-24997-1

Fracture Mechanics

Perez, N.

2017, XIV, 418 p. 205 illus., 179 illus. in color.,
Hardcover
ISBN: 978-3-319-24997-1